The LCLS-II Photo-Injector Drive Laser System

Sasha Gilevich, Shawn Alverson, Sergio Carbajo, Stefan Droste, Steve Edstrom, Alan Fry, Michael Greenberg, Randy Lemons, Alan Miahnahri, Wayne Polzin, Sharon Vetter, Feng Zhou
SLAC National Accelerator Laboratory, 2575 Sand Hill Road, Menlo Park, CA 94025, USA
Gilevich@slac.stanford.edu

Abstract: We present the new drive laser system for the LCLS-II free electron laser photo-injector, including the first commissioning results and challenges encountered due to high power, high repetition rate ultraviolet laser operation.

1. Introduction

The Linac Coherent Light Source (LCLS) has been a fully operational X-ray Free Electron Laser (XFEL) user facility since 2009, operating at 120Hz repetition rate [1]. Construction of the second XFEL is underway at SLAC, namely LCLS II, that will be operating at the higher repetition rate – adjustable up to 1MHz. An essential component of the LCLS-II XFEL is the Injector Drive Laser system, which is used to produce photoelectrons for the linear accelerator. This laser system produces ultraviolet (UV) pulses that illuminate a photocathode located inside a high-field radiofrequency (RF) gun, i.e. the photo-injector, to generate a high-quality electron beam [2,3]. The main target parameters for the UV beam on the cathode are presented in Table 1:

Table 1. Required laser beam parameters on the cathode

Parameter	Nominal value	Min	Max	unit
Operating wavelength	257.5	-	-	nm
Pulse repetition rate	0.625	0	0.928	MHz
Energy per pulse	0.1	0	0.3	µJ
Beam size on cathode (FWHM)	0.8	0.2	2	mm
Pulse duration	30	20	60	ps
Temporal Shape	Flat top with maximum 2 ps rise/fall time			
Spatial Shape	Apodized Gaussian or uniform (flat top)			

Commissioning of the RF gun is currently ongoing, and the first electrons were produced in May 2019. The required laser beam parameters, in particular the combination of sufficient UV pulse energy and temporal-spatial shaping, imposes substantial challenges that are currently addressed through an independent R&D effort. In this paper, we describe the LCLS II Injector Laser system, including the laser, UV conversion unit and transport. We discuss the problems that we encountered, solutions that we have implemented and our plans moving forward.

2. The Injector Drive Laser System

A block diagram of the Injector Drive Laser System Drive Laser system is presented in Figure 1.

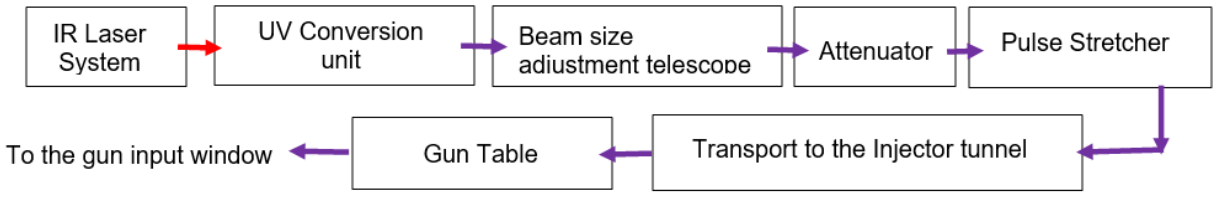

Figure 1. Block Diagram of the Drive Laser System

2.1 IR Laser System

The infrared (IR) front-end system is a commercial laser manufactured by Amplitude Systemes. It is comprised of Ytterbium-based oscillator operating at 46.43MHz, fiber stretcher, fiber preamplifier, pulse picker, diode-pumped fiber amplifier (Tangerine [4]), acousto-optics modulator, that controls the laser system output repetition rate, and adjustable compressor. The oscillator is phase-locked to the accelerator RF reference system. The laser system includes a Finisar WaveShaper [5], a programmable spectral phase and amplitude shaper that allows spectrum manipulations and can be of assistance for the purposes of temporal shaping. The laser system also features a short pulse module, capable of producing pulses with a duration of ~ 50 fs (FWHM), and ~100 mW power, at a center wavelength of 1030 nm and repetition rate of 46.63MHz. It is used for temporal shape diagnostics via optical cross-correlation. Altogether, the IR front-end produces 50 µJ, 1030 nm pulses with adjustable repetition rate up to ~1MHz and an adjustable pulse duration from ~330 fs to 30 ps.

Block diagram of the IR front-end laser is shown on Figure 2.

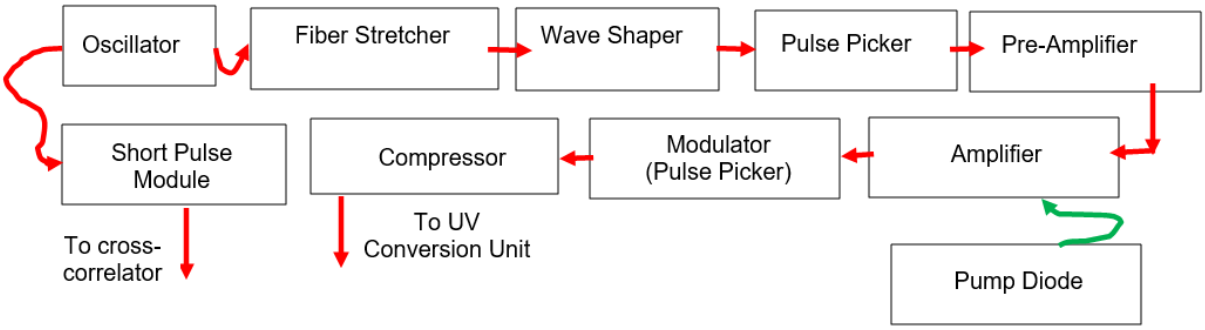

Figure 2. Block Diagram of the front-end IR Laser System

2.2 IR –UV Conversion

For the IR-to-UV conversion, we employ two frequency-doubling stages to convert the 1030 nm laser output to 515 nm and further to 257.5 nm. The first frequency-doubling is achieved in a 3 mm long beta barium borate (BBO) crystal that generates the second harmonic (SHG) at 515 nm, while the second doubling stage uses a 1 mm long BBO crystal to produce the fourth harmonic (FHG) at 257.5 nm pulses required for the photoemission. The FHG crystal is placed in a temperature-regulated enclosure.

For temporally-compressed (nearly transform limited) IR pulse SHG, we achieve a conversion efficiency between 50 – 65% and a FHG conversion efficiency from IR to UV of about 10 to 20%. The variations are associated to different repetition rates and thus thermal load onto both SHG and FHG crystals.

While compressed IR pulses yield the highest conversion efficiency and the shortest pulse duration in the UV, the LCLS-II design beam parameters require UV pulses with increased temporal durations (see Table 1). Introducing a chirp to the IR beam in a traditional collinear SHG and FHG stage resulted in severe temporal intensity modulations in the UV beam and yielded insufficient conversion efficiency (<5%). Therefore, our commissioning phase approach involves FHG using the fully compressed IR beam and stretching the maximum available UV bandwidth with a Treacy type 2-pass reflective grating stretcher [6]. The stretcher path length is adjustable to vary the pulse duration in the present configuration from 10 to 30 ps, (see Figure 3.)

It is important to note that this configuration does not meet the flat-top temporal shape requirements and produces instead a Gaussian-like temporal profile of the UV pulses.

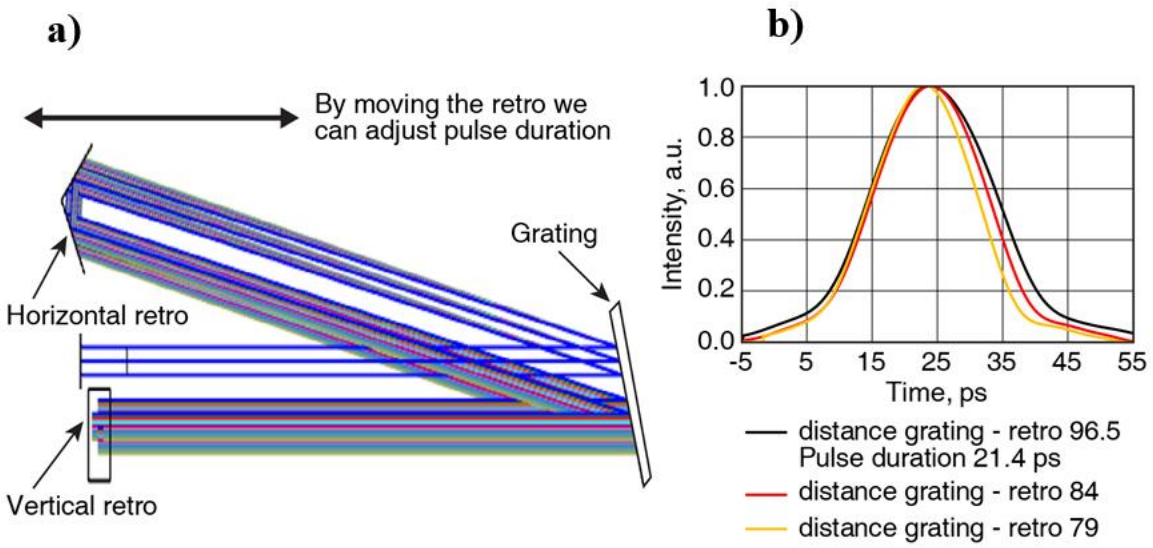

Figure 3. a) Schematics of the UV stretcher and b) pulse shapes for three different stretcher settings with different distances (in cm) between grating and retro

The first-order efficiency of the 3600 groves per mm grating is about 80%, yielding about 40% transmission through the stretcher. In order to increase transmission through stretcher we are looking at the possibilities to use gratings that are more efficient. Using transmission gratings that unlike reflection UV gratings do not have metallic coating that absorbs UV beam, might be a solution. However, in the case of transmission gratings durability of the substrate is very critical, especially in the high-power environment.

The high laser power, substantial UV absorption, and low thermal conductivity of BBO leads to severe thermal management challenges in the FHG crystal. At repetition rates above 100 kHz, we originally observed very unstable (more than 70% power drops) UV power, poor beam quality and strong thermal lensing. We resolved this problem by carefully optimizing the beam size of the SHG light in the FHG crystal for each average power level. The smaller beam size should result in higher conversion efficiency, but on the other hand, it will lead to more severe thermal management problems. Thus, a tradeoff must be found. To adjust the beam size, we use a 3-lens zoom telescope. We use 250 mm focal length plano-convex lenses as the first and third telescope lenses and one -75 mm focal length plano-concave lens as the second one. By changing the distances between the first and second lenses, we control the beam size, and by adjusting the distance between the second and the third lens keep the beam collimated.

The UV pulse energy is shown in Fig. 4.a for three different SHG beam diameters at the higher repetition rate of 928 kHz. At the power levels below ~ 5.5 – 6W a smaller beam size generates higher UV pulse energy, but at higher UV power when the thermal issues begin to affect the FHG process all three beam diameters lead to about the same pulse energy.
Fig. 4.b shows IR to UV conversion efficiency and Fig. 4.c shows the transverse beam shapes. Decreasing the beam size at the certain UV power levels leads to distortion in the spatial beam shape and decrease of conversion efficiency. The optimum beam size for each power level should be found. Thermal effects in the FHG crystal limit the achievable output pulse energy as can be seen from the dashed curved in Fig. 4A and 4B that shows the UV pulse energy at a repetition rate of 92.8 kHz.

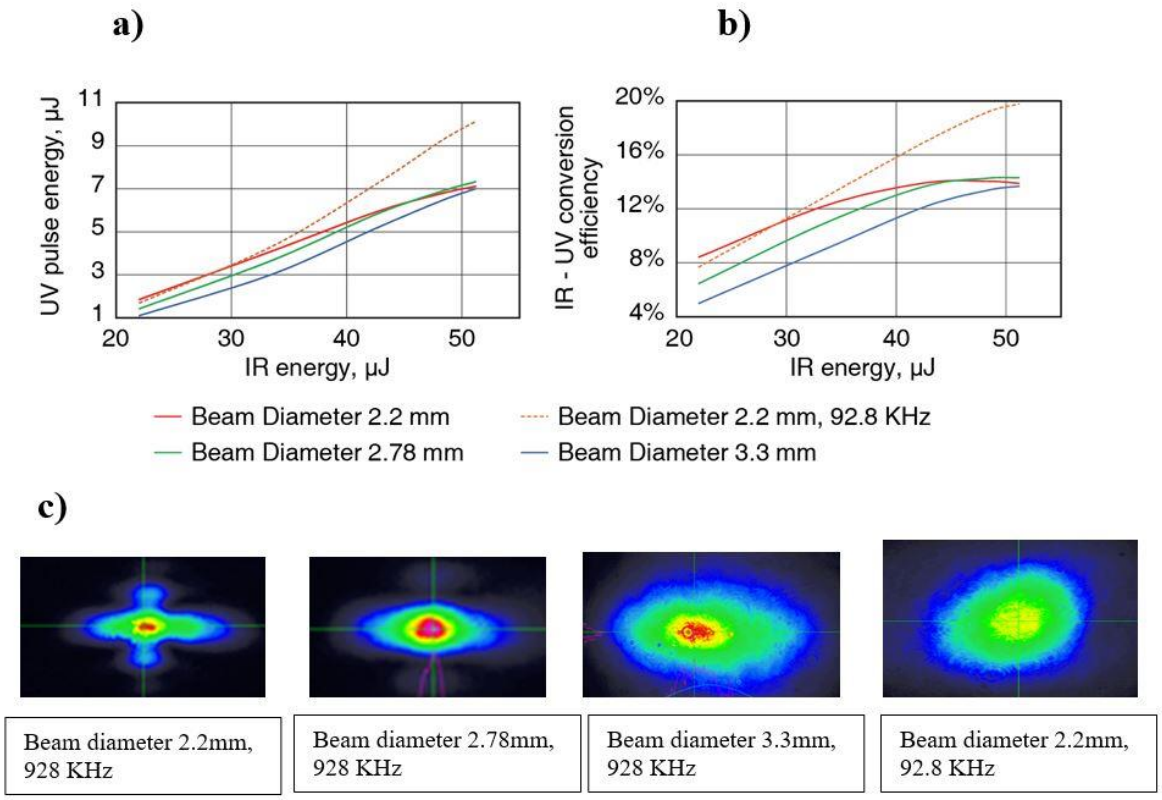

Figure 4. a) UV pulse energy and b) IR-UV conversion efficiency for different SHG beam diameters in the FHG crystal at 928 kHz repetition rate. For comparison, the UV pulse energy and conversion efficiency at 92.8 kHz is shown as well. C) UV beam profile for the three SHG beam diameters.

For repetition rates below 100 kHz and the SHG beam diameters below 2.8 mm, the UV conversion efficiency is reported to be significantly higher compared with the repetition rates above 100 kHz. For larger SHG (and consequently UV) beam sizes, when thermal effects play lesser role due to better heat extraction, UV conversion efficiency remained about the same. For lower repetition rates it was possible to achieve better conversion efficiency by reducing the beam size, see Fig. 5.

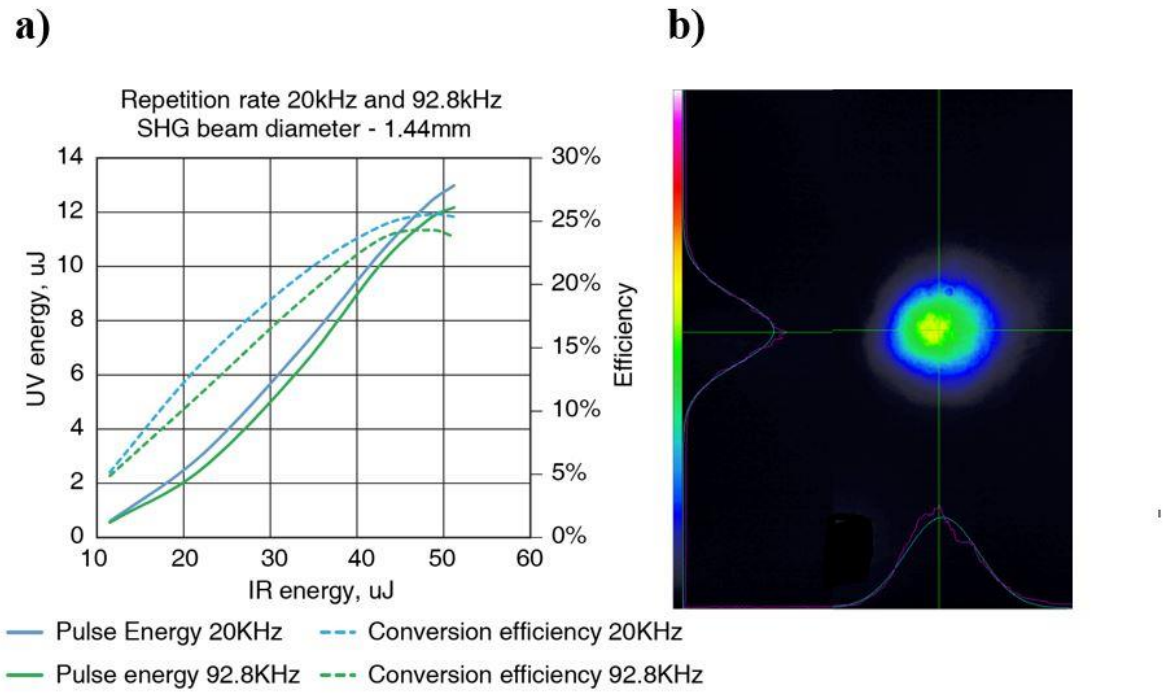

Figure 5. a) UV Pulse energy and conversion efficiency versus input IR pulse energy for SHG beam diameter 1.44 mm. b) UV beam spatial shape at 92.8 KHz

As shown above, the different thermal loads in the FGH crystal due to different repetition rates can be managed by adjusting the SHG beam diameter. With a beam diameter from about 1.5mm (for repetition rate <20 kHz) to 2.8mm (for 1 MHz), we had achieved stable power levels up to ~6W (1 MHz) and Gaussian transverse shape through all required repetition rates. However, at repetition rates exceeding 300 kHz a compromise between thermal stability, adequate spatial quality and conversion efficiency had to be found. In this high repetition rate regime, we found an adequate compromise sacrificing the conversion efficiency by about 20 % relative to the highest achieved, which still meets power requirements on the cathode.

3. Laser Transport

The RF gun is located in a radiation-shielded area at the beginning of the LCLS-II injector tunnel while the drive laser system is installed in an adjacent laser room. Therefore, the UV light has to be transported over a total distance of about 20 m through evacuated transport tubes.

The output plane of the laser system (downstream of the zoom telescope) is imaged onto a transverse beam-shaping aperture located on the RF gun table by a two-stage relay system with demagnification 4:1. The turning mirrors and relay lenses are located in evacuated boxes, which together with the transport tubes form a unified vacuum system. The transverse beam shaping aperture is imaged onto the cathode with 2:1 demagnification, which creates an apodized Gaussian or uniform transverse beam shape on the cathode surface by overfilling the aforementioned aperture. The transport system also includes a three-lens zoom telescope that enables beam size adjustments on this aperture and a beam attenuator that consists of a half-wave plate and polarizer and is located after the zoom telescope.

The transport system employs a “virtual cathode” concept, i.e. a camera placed in the equivalent to the cathode plane that allows monitoring the beam position and its spatial shape on the cathode. The virtual cathode and an additional camera are used for a feedback loop that maintains the beam position and pointing on the photocathode and inside the gun. The schematics of the beam transport, including gun table optical setup is presented on Fig 6.

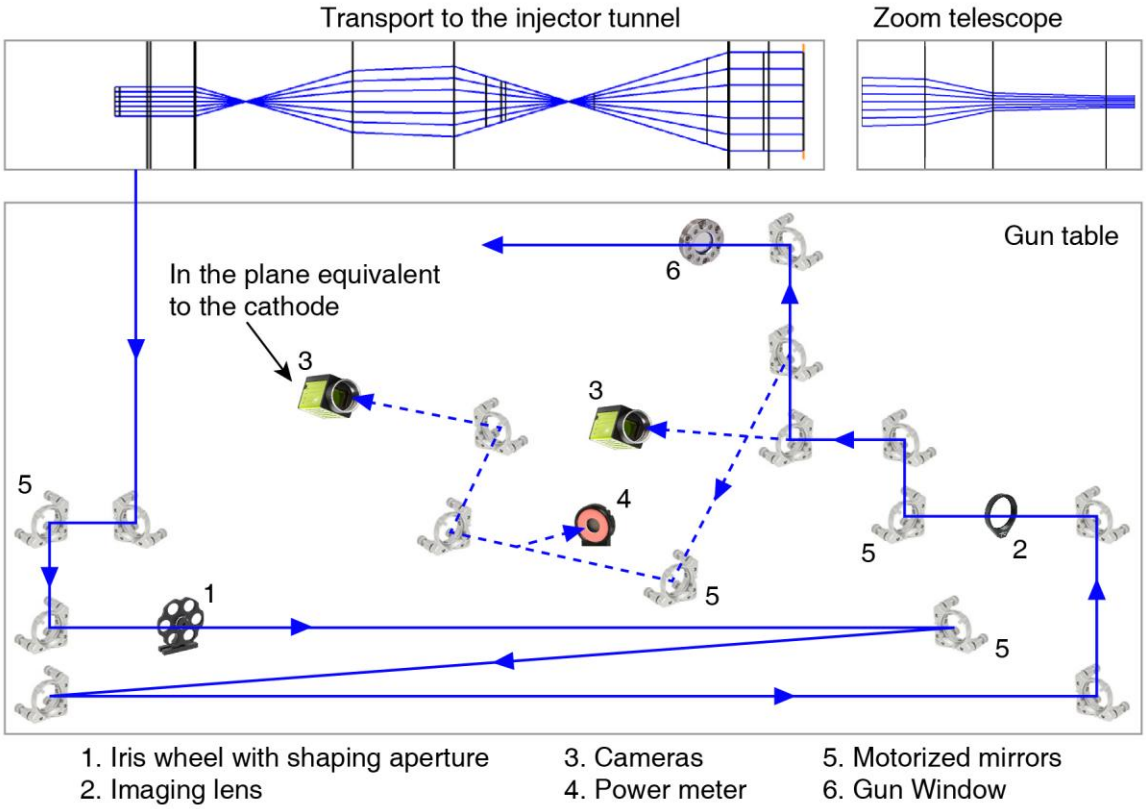

Figure 6. Laser Beam Transport

The UV generation, spatial and temporal shaping as well as the beam transport introduce high losses, which are summarized in Table 2.

Table 2. Transmission through the transport

Device	**Transmission**	**Comment**
UV Conversion Unit	10 – 22%	Conversion efficiency depends on repetition rate
Beam splitters for diagnostics	85%	
Attenuator	92%	Transmission through optical components goes down after a certain UV exposure time due to contamination
Stretcher	40%	
Transport to tunnel	80%	
Transverse shaping aperture	30%	Transmission through the shaping aperture depends on the required beam size and the spatial shape

Transmission through the transport was only about 80% that was most likely due to fluorescence in the transport optics, which were manufactured from UV grade fused silica. We are hoping to increase this number by using the better optics' material (see the next section) and if necessary, by increasing the beam size on the transport optics.

4. Optics Degradation Test

UV beam delivery at the few-W average power level imposes a critical operational dependency on the performance and durability of the optics for future 24/7 facility operations. We have been carrying out long term

tests of different UV optical materials to examine the evolution of their performance under continuous Watt-level UV power. The lifetime of the optics depends on power level, size and the spatial shape of the illuminating beam. The examples of our tests' results are presented in the tables below.

The following materials have been tested:

Material 1: UV grade regular fused silica – Uncoated (OH content 800 – 1000 ppm). Although we didn't observe any significant transmission degradation at the duration of our tests (tens of hours), we observed significant degradation of the spatial beam quality most likely due to material damage and color centers formation [7, 8], (see fig.9). The examples of the tests results are presented in the Table 3.

Table 3. Selected Results for UV grade regular fused silica:

Power density, W/cm2	Test duration, hours	Results	Comments
120	18	Complete deterioration of the spatial shape	See Fig1; A)
80	24	Spatial shape started to deteriorate	See Fig 1; B)
61	72	Complete deterioration of the spatial shape	See Fig 1; C)
27	192	Start of the color centers formation	See Fig 1; D)
13	157	No noticeable spatial shape degradation	

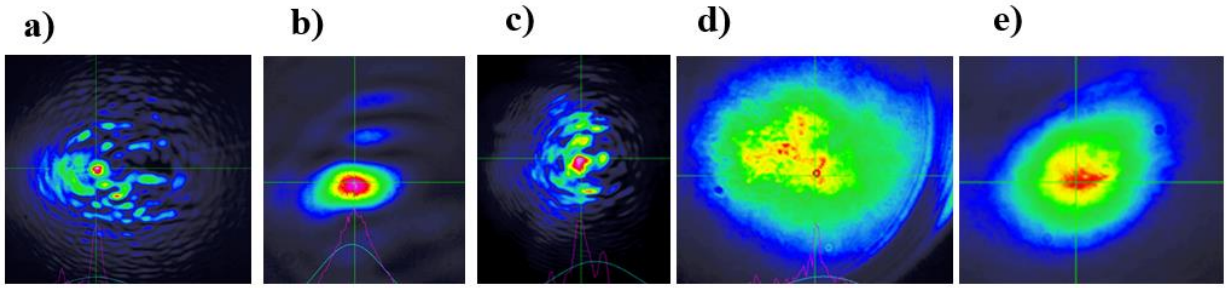

Figure 7. Spatial shapes of the laser beam transmitted through UV grade fused silica samples.

a)122W/cm2 after18 h; **b)** 80W/cm2 after 24 h; **c)** 61W/cm2 after72 h; **d)** 27W/cm2 after 192 h; **e)** Example of the input beam spatial shape

Material 2: Corning fused silica 8655. It is higher purity - with <1ppm of OH content non-crystaline silica glass. As expected, in this case we observed longer durability than in regular UV grade fused silica case – see Table 4. We have tested uncoated Corning fused silica 8655 as well as the samples with nano-textured anti-reflection structure [9]. Durability of both types of samples was about the same. We found AR nano-texturing technology very promising and are planning to use it for the beamline transport refractive optics.

Table 4. Selected Results for the Corning 8655 fused silica:

Power density, W/cm2	Test duration, hours	Results	Comments
120	24	Surface damage	
80	75	Complete deterioration of the spatial shape	See Fig 2; A)
60	116	Spatial shape started to deteriorate	See Fig 2; B)
18	168	No noticeable spatial shape degradation	

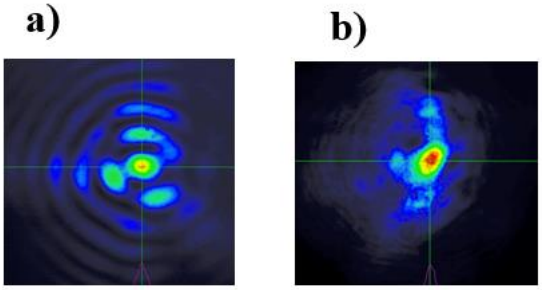

Figure 8. Spatial shapes of the laser beam transmitted through Corning 8655 fused silica samples

a)79.5W/cm2 after 75 hour; **b)** 61.4W/cm2 after 116 hours

Material 3: CaF2 – LD – laser durable calcuim fluoride provided by Corning. None of our tests resulted in any noticeable transmission or spatial shape of transmitted beam degradation. Our tests demonstrated that regular UV grade fused silica supplied by most manufacturers can not provide in our case operationally acceptable durability. For a power density level not exceeding a certain amount Corning fused silica 8655 could be used. But the best material for the high power laser transport optics is laser durable CaF2.

Table 5. Selected Results for Corning 8655 fused silica:

Power density, W/cm2	Test duration, hours	Results	Comments
120	24	No noticeable spatial shape degradation	
80	216	No noticeable spatial shape degradation	

Fluorescence spectra of the tested materials and regular CaF2, when illuminated with the laser UV beam, are presented on Fig.9

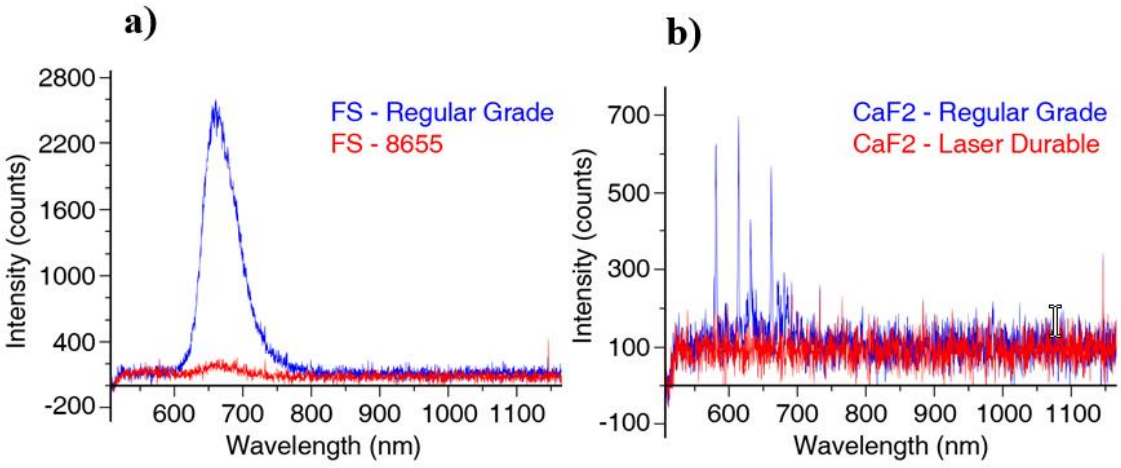

Figure 9. Fluorescence spectra of a) regular grade and Corning 8655 fused silica and b) regular grade and Laser Durable CaF2

5. Conclusion

We presented the new photo-injector drive laser system for SLAC LCLS-II XFEL, which is now undergoing commissioning. We have achieved laser pulse energy on the cathode of 0.3μJ at the repetition rate up to 1MHz with

the beam diameter 1mm, the spatial shape close to Gaussian cut, the temporal shape ~ 20ps long Gaussian pulse. It allowed us to get 300pC charge from a Cs_2Te cathode.

Our future work will be concentrated on achieving the laser system durability and stability that can ensure stable 24/7 operation. We are planning to replace critical optics made of UV grade fused silica by CaF2 – LD and Corning 8655 fused silica one and to use AR nano-texture treated materials. Another aspect of our future work will involve advanced spatio-temporal pulse shaping.

6. References

[1] Christoph Bostedt, et el., "Linac Coherent Light Source: The first five years", Rev. Mod. Phys. **88**, 015007
[2] J.F. Schmerge, et el., "The LCLS II Injector Design", Proceedings of the 36th Int. Free Electron Laser Conf. (FEL'14), paper THP042
[3] Stohr, J. Linac coherent light source II (LCLS-II) conceptual design report. No. SLAC-R-978. SLAC National Accelerator Lab., Menlo Park, CA (United States), 2011.
[4] https://amplitude-laser.com/produit/tangerine/
[5] https://www.finisar.com/sites/default/files/downloads/waveshaper_1000sp_product_guide_web_april_2016.pdf
[6] E. B. Treacy, "Optical pulse compression with diffraction gratings", IEEE J. Quantum Electron. 5 (9), 454 (1969)
[7] T. E. Tsai, D. L. Griscom, and E. J. Friebele, Mechanism of Intrinsic Si E'-Center Photo generation in High-Purity Silica. Phys. Rev. Letters, v **61**, # 4, 444, (1988)
[8] https://www.photonics.com/Articles/Assessing_Damage_for_UV-Laser-Resistant_Fused/a12306
[9] Update on the Development of High Performance Anti-Reflecting Surface Relief Micro-Structures - Hobbs, D.S., MacLeod, B.D., and Riccobono, J., Proc. SPIE **6545**, 65450Y (2007) Windows and Domes